Low cost, high performance spray pyrolysis grown amorphous Zinc Tin Oxide: The challenge of a complex growth process

Supplementary Information

Ainur Zhussupbekova,*,† David Caffrey,† Kuanysh Zhussupbekov,† Christopher M. Smith,† Igor V. Shvets,† and Karsten Fleischer†

†*School of Physics and Centre for Research on Adaptive Nanostructures and Nanodevices (CRANN), Trinity College Dublin, Dublin 2, Ireland*
‡*School of Physics, Dublin City University, Dublin 9, Ireland*

E-mail: zhussupa@tcd.ie

1 XPS analysis

In this work the composition of amorphous zinc-tin oxide (a-ZTO) was determined via X-ray photoelectron spectroscopy (XPS) by analysing the intensity ratios of the Sn $3p^{3/2}$ vs. the Zn $2p^{1/2}$ core levels. XPS is a surface sensitve technique with the electron escape depth varying between 5-10 nm depending on the kinetic energy of the photoelectron. As samples are grown in atmosphere from organic precursors, there is a adlayer of organic molecules and hydroxides, which can substantially alter the determined Zn/Sn ratio as the Sn probe depth is about 1.7 times larger than the Zn probe depth. A closed layer of adsorbates will therefore attenuate the Zn signal much more than the Sn signal.

The removal of these organic adsorbates within the UHV system is required for a reliable determination of the stoichiometry. The method of choice is Ar ion etching. This ion etching in itself can alter the measured stoichiometry if specific cations are sputtered preferentially during the process. Therefore, sputter conditions and etching times have be carefully chosen to a) remove the adsorbates and b) minimise actual etching of the thin film.

We established that Ar-etch with acceleration voltages much less than 1 kV is the most reliable sputtering procedure for our experimental setup. Previous measurements on thick films of doped ZnO, $CuCrO_2$, $SrTiO_3$, and TiO_2 have shown that our standard process of 10 min Ar etching with 750 V acceleration voltage, 6 μA ion current, at 1.5×10^{-3} Pa Ar pressure is sufficient to remove organic adsorbates, while not substantially etching the film itself. Nevertheless, to eliminate a possibility of preferential Zn or Sn sputtering that can alter composition we investigated an effect of Ar sputtering on the films stoichiometry. Figure S1 shows XPS measurements of a-ZTO sample as grown, after one, and after two such cleaning cycles. The first cycle was sufficient to remove all residual carbon, while a second cycle only slightly changes the determined stoichiometry. We therefore applied exactly the same cleaning cycle to all samples without any changes to the process. There is no evidence of preferential sputtering as this would reduce the signal from lighter elements such as Zn and O compared to the heavier Sn cation. The difference in x_{film} seen between the first and second sputter cycle was also used to estimate the error of the determination of x_{film}.

2 X-Ray diffraction

Crystallographic structure of the films are investigated employing a Bruker D8 Advance X-ray diffraction system with a Cu Kα X-ray source.

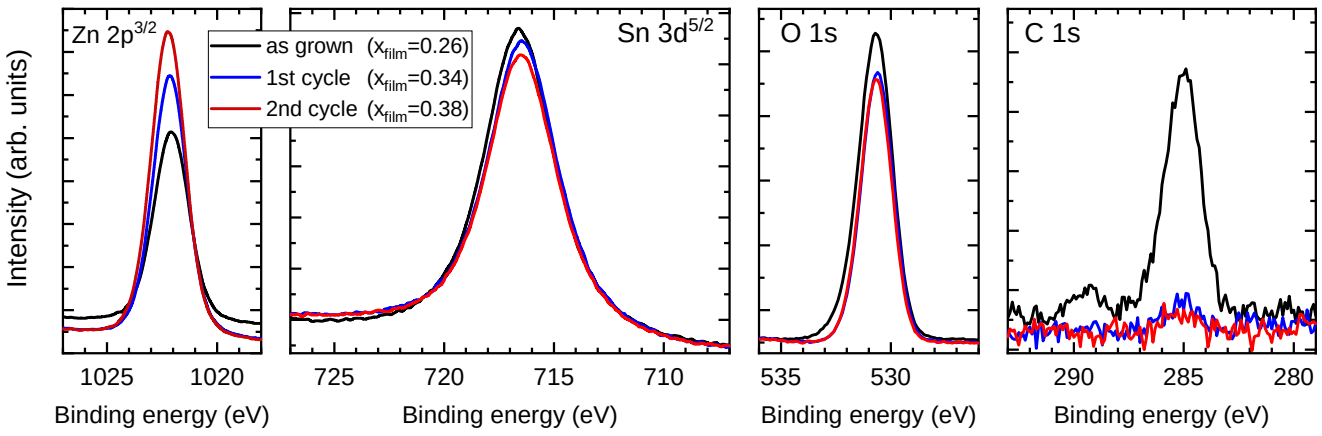

Figure S1: XPS raw measurements for an a-ZTO sample after transfer into the UVH system, a 10 min Ar-etching cycle (0.75kV, 6 μA, 1.5×10^{-3}Pa) and a second subsequent etching with the same conditions. The standard 10 min cycle is sufficient to remove the organic adsorbates. Further etching doesn't alter the residual Carbon signal from areas screened from the ion beam (fissures, cracks, shadowed areas in rough samples). The Carbon removal is accompanied by an increase in the Zn counts, most attenuated by overlayers. The Zn content in the film (x_{film}) is calculated from area fits of the entire core level. As the Zn peak is very sharp and has a higher sensitivity factor compared to the Sn 3d core level, the calculated change in x_{film} is less than the raw peak amplitude change would suggest.

Films with varying x_{film} compared to background signal from the glass substrate and sample holder. In order to increase film/substrate ratio X-ray diffraction measurements were performed in a grazing incidence (GIXRD) regime. However, a small contribution of the underlying glass substrate at 48-50° is still present in films. Despite having various stoichiometry all films demonstrate broad amorphous 'halo' structure without crystalline features. Some difference in the intensity of the signal between the films is assigned to the thickness variation. The only notable exception being film x_{film}=0.25, highest Sn content among the set, that display a SnO_2 (101) and (211) peaks due to fragmentary de-phasing of the film. These reflexes indexed in Figure S2.

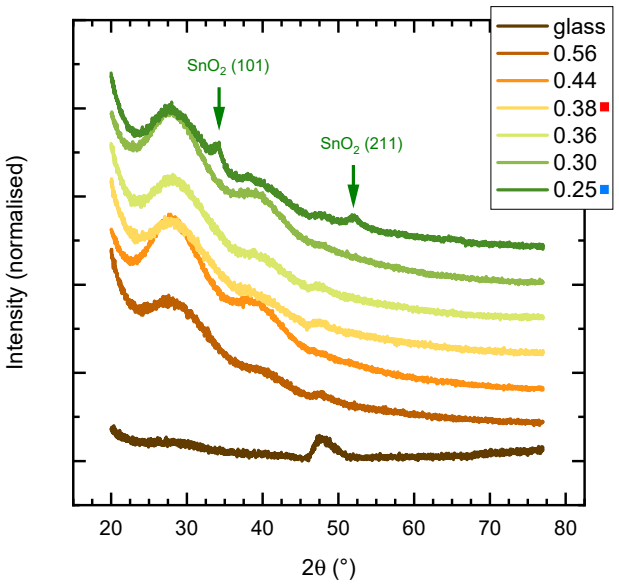

Figure S2: GIXRD data for sample with varying x_{film}. Only very broad structures are seen caused by incoherent scattering and increased roughness. The most Sn-rich sample shows some SnO_2 reflexes in addition to the broad amorphous structure indicating a partial de-phasing of the film.

3 AFM measurements

Atomic force microscopy (AFM) measurements were conducted on an Asylum MFP-3D microscope with AC Air Topography mode to quantify morphology difference in the films and gain insight into topography. The scanning was performed at 300 kHz frequency utilising rectangular cantilevers with tetrahedral tips from Oxford In-

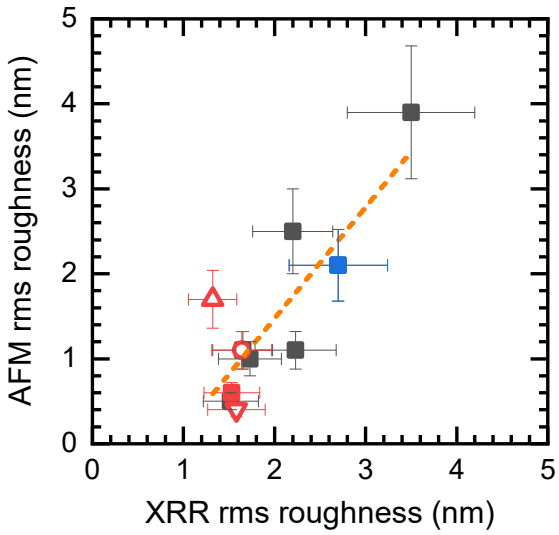

Figure S3: Comparison of local AFM based roughness ($1\times1\,\mu m^2$ area) with the rms determined from XRR fits on the entire sample. While the numerical values differ, the overall trend is in agreement

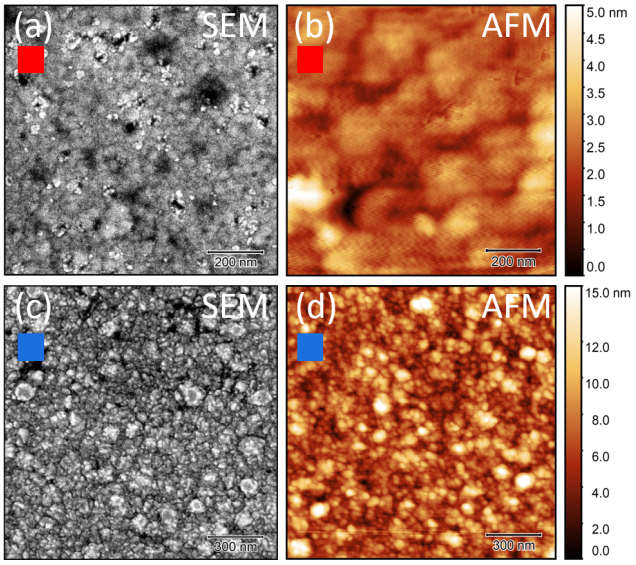

Figure S4: (a) and (b) SEM and AFM images of the film with the highest conductivity of 304 S/cm and mobility value of 10 cm^2/Vs. (c) and (d) SEM and AFM images of the film x_{film}=0.25 exhibiting the presence of SnO_2 crystallites on GIXRD. Note there is a factor of 3 in the height scale between the smooth x_{film}=0.38 and rough x_{film}=0.25 sample.

struments.

The topographic profile of the films measured via AFM allows to obtain values of local roughness on the scanned area as its directly registers the surface profile with nanometer resolution, while XRR measurements reveal roughness information with a density profile from the entire thin film. Despite the fact that AFM probes locally, roughness's obtained by AFM are broadly following the same trend as measured by XRR (see Figure S3).

AFM and XRR tools cover different ranges of lateral spatial frequency and probing depth, therefore the surface roughness measured by these two methods is not always compatible, especially taking into account surface contamination present in SP grown samples. The comparison of the SEM image with AFM image (Figure S4(a) and (b)) for film with the highest conductivity demonstrates that the small cracks present in SEM as a contrast modulation are not observable via AFM as usage of 20 nm radius tip does not allow resolve few nm scale cracks.

However, the for the film with x_{film}=0.25 that displays SnO_2 crystallites on GIXRD and larger grain size a strong correlation between the SEM and AFM images can be observed (Figure S4(c and d)). Both AFM and SEM techniques showed the same range of grain sizes from 20 nm to 100 nm. Some brighter clusters on the SEM image can be attributed to SnO_2 crystallites observed in the GIXRD. It is also seen that this film with the highest Sn content is significantly rougher than the optimised film exhibiting the highest conductivity.